Influence of size and shape on key performance metrics in spin-torque oscillators

Cite as: AIP Advances **11**, 025215 (2021); https://doi.org/10.1063/9.0000230
Submitted: 15 October 2020 . Accepted: 20 January 2021 . Published Online: 05 February 2021

Brandon R. Zink, Yang Lv and Jian-Ping Wang

Influence of size and shape on key performance metrics in spin-torque oscillators

Cite as: AIP Advances 11, 025215 (2021); doi: 10.1063/9.0000230
Presented: 4 November 2020 • Submitted: 15 October 2020 •
Accepted: 20 January 2021 • Published Online: 5 February 2021

Brandon R. Zink,[a] Yang Lv, and Jian-Ping Wang[a]

AFFILIATIONS

Department of Electrical and Computer Engineering, University of Minnesota, Minneapolis, Minnesota 55455, USA

Note: This paper was presented at the 65th Annual Conference on Magnetism and Magnetic Materials.
[a]**Authors to whom correspondence should be addressed:** zinkx030@umn.edu and jpwang@umn.edu

ABSTRACT

Spin Torque Oscillators (STOs) are promising solutions in a wide variety of next generation technologies from read-head sensors in high-density magnetic recording technology to neural oscillator units for neuromorphic computing. There are several metrics that can be used to quantify the performance of an STO such as power, quality factor, frequency tunability, etc., most of which are dependent on the design of the STO device itself. Furthermore, determining the most important metric will be contingent on its desired application, meaning that it is crucial to understand how the STOs design parameters influence all aspects of its performance so that its design can be optimized to perform the desired function. In this work, we analyzed spin torque oscillations generated from 20 magnetic tunnel junctions with in-plane anisotropy and patterned into elliptical nano-pillars with a wide range of sizes and aspect ratios. For each device, we acquired 20 to 50 data sets at various bias fields and currents and used power spectral density plots to measure output power, frequency, linewidth, quality factor, and power-to-linewidth ratio for each set. We also analyzed each STOs performance in terms of the bias fields and bias currents required to maximize output power and signal quality as well as the frequency tunability with both field and current. By comparing all of these performance metrics between the 20 STOs tested, we studied the influence of device size and shape on all aspects of STO performance and used correlation coefficients to quantify relative magnitude of these effects.

I. INTRODUCTION

Spin-torque oscillators (STOs) are nanoscale, ferromagnetic devices capable of generating self-sustained, high frequency signals, which are caused by stable magnetization precessions induced by a spin polarized current via the spin transfer torque (STT) effect.[1–6] Implementing STOs in modern technologies is challenging since the output power and quality factors of their signals are several orders of magnitude lower than needed for modern applications.[1–6] Nevertheless, STOs exhibit many unique and novel properties such as nonlinearity, frequency tunability and synchronization[7] which give them exciting prospects for next generation computation, communication, and sensor technologies.

Experimental work performed over the last decade has demonstrated that the frequency in STOs can be tuned over several GHz using external DC biases such as a magnetic field and an electrical current.[8] This feature has led to various studies which propose STOs as the working principal in wireless on-chip and chip-to-chip communication technologies[9,10] as well as new sensor technologies such as STO-based read-head sensors in high density magnetic recording arrays[11,12] and bio detection systems.[13] Additionally, STO frequencies can be synchronized to an external source, which includes either an RF field[14] or an RF current through injection locking[15] or to other STOs through mutual coupling. STO coupling can be done via spin wave propagation,[16] dipole interactions,[17] or electrical coupling, which is caused by self-modulation of the current through each STO.[18] Not only is this feature is a promising solution for enhancing output power and quality of STO signals,[15–18] but it has also made STOs a promising solution in a novel next generation computing paradigm where large scale oscillator arrays mimic neural activities for bio-inspired functions.[19–22]

There are numerous metrics that can be used to quantify the performance of an STO, many of which are independent on one another. Determining which of the metrics is the most important is

dependent on the desired application which is why it is important to understand how the intrinsic properties of the device influence each of these performance metrics so that STO designs can be optimized for the desired function. Simulations in OOMMF have shown that when the STO size decreases from 40 x 40 nm^2 to 10 x 10 nm^2, then the linewidth increased approximately three-fold and the frequency is reduced by almost 0.8 GHz.[23] X. Chao *et al.*[24] studied the influence of shape anisotropy on the STOs signal quality and demonstrated that the quality factor of the signals generated by STOs improved ~1.5X as the STOs coercivity increased from 60 Oe to 170 Oe. However, it is not clear if the STOs signal quality has a stronger dependence on STO size or shape anisotropy as well as the effects that these two parameters have on other STO performance metrics.

In this work, we study spin-torque oscillations generated from 20 MgO-based magnetic tunnel junctions (MTJs) and their dependence on both device size and shape. We characterized the output signals generated from these MTJs by 12 different performance metrics which include output power, precession frequency, linewidth, quality factor, the bias field and current required to optimize STO performance, and the change in frequency with both bias field and bias current. The relative strength of each of these metrics was quantified with respect to STO size and shape using correlation coefficients. By studying all aspects of the STOs performance, our study provides a basis for application-specific optimization of future STO designs.

II. EXPERIMENT

There were 20 MTJs tested with varying sizes and aspect ratios (long-axis/short-axis lengths). For the complete stack structure of the MTJs and descriptions of each device tested, see supplementary material, note 1 and supplementary material, Table I. However, some of our MTJs had similar nominal dimensions but had significantly different field switching behavior, which illustrates that the actual device dimensions may have varied from their nominal dimensions. To compensate for these variations in our analysis, we represented the STOs size and shape by their measured P-state resistance (R_P) and the coercivity (H_C) respectively, which were measured from field switching (R-H) hysteresis plots (see supplementary material, note 2 and supplementary material, figure 1).

Spin-torque oscillations were generated through the application of an applied bias field (H_{bias}) and a DC current bias (I_{bias}), which favor opposing states. The output RF signals were transmitted through a microwave probe which were isolated from the DC component using a bias tee. These signals were amplified by +27 dB then measured using a Tektronix DPO 72004C mixed signal oscilloscope with a sampling rate of 50 Gs/second. The STO waveforms acquired were analyzed using power spectral density (PSD) plots, an example of which is shown in Figure 1a. For each data set, we found precession frequency (f_p), and linewidth (Δf) by fitting the first harmonic peak to a Lorentzian curve, as illustrated in the example in Figure 1b. From these measurements, we calculated the quality factor (Q_f) of the signal, which is defined as $f_p/\Delta f$. Lastly, output power (P_{out}) was also be obtained by integrating the PSD curve through the entire frequency bandwidth.

In addition to P_{out}, f_p, Δf, and Q_f, we also investigated the influence of R_P and H_C on the H_{bias} and I_{bias} values required to generate the precession signals for each STO. Note that most of the STOs tested had an intrinsic stay field (H_{stray}), which is represented as the offset in the R-H hysteresis curve along the x-axis, an example of which is shown in Figure 1c. Note that H_{stray} = -35 Oe in Figure 1c, however, each STO had a different H_{stray}. For valid comparison between STOs, we defined H_{bias} as $H_{bias} = H_{appl} + H_{stray}$, where H_{appl} is the applied field.

In our analysis, we compared each of these performance metrics between all STOs tested in order to determine their dependence on device size and aspect ratio. Note that each STO tested contained between 30 and 50 data sets, each with different bias conditions, so to make valid comparisons between STOs, we defined the top 8 data sets for each STO and calculated averages for P_{out}, f_p, Δf, Q_f, H_{bias} and I_{bias} measurements among these sets. This way, we are only comparing these performance metrics in the sets with optimum performance. A challenge faced with this approach is that it is not clear how to define the 'best' sets because the criteria for 'best' is likely to be application dependent. To avoid this problem, we analyzed our results using two independent methods of defining the top data sets: 1) Sets ranked by P_{out} and 2) sets ranked by Q_f. To analyze the relation of each metric with STO size and shape, we plotted P_{out}, f_p, Δf, Q_f, H_{bias} and I_{bias} with R_P and H_C separately. The magnitude of the dependence of R_P and H_C on each performance

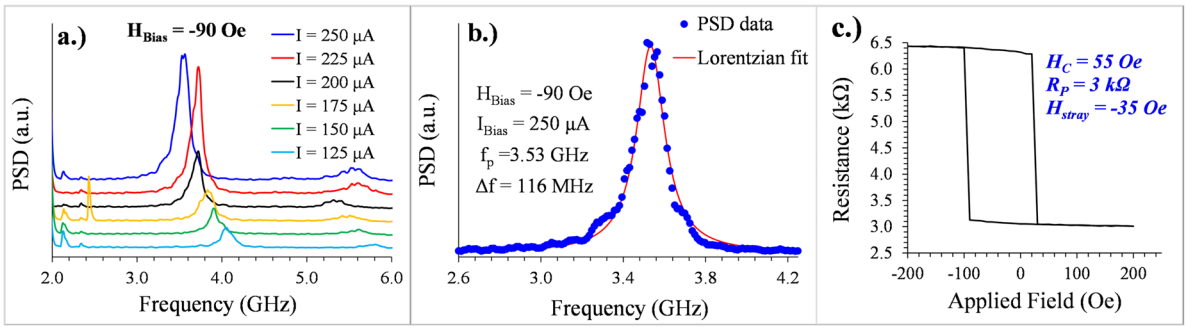

FIG. 1. Example of power spectral density plot from STO 13 (see supplementary material, Table I) at a bias field of −90 Oe a.) spectral densities at various bias currents (I_{bias}), b.) Lorentzian fit on the I_{bias} = 250 μA data set, from which, precession frequency (f_p) and linewidth (Δf) can be obtained and c.) R-H hysteresis plot used to obtain critical intrinsic device properties key for our analysis.

metric was quantified using their linear correlation coefficients (ρ). Note that it is unlikely that all seven metrics studied actually have linear relationships with R_P and H_C, so ρ simply serves as a factor to quantify the relative dependencies on R_P and H_C but does not necessarily indicate linear relations. For further details regarding our error analysis of ρ as well as all plots used to calculate ρ values, see supplementary material, note 3 and supplementary material, Figures 2–4.

III. RESULTS AND DISCUSSION

Figures 2a–b show the linear correlation coefficients (ρ) for P_{out}, f_p, Δf, Q_f, H_{bias} and I_{bias} with R_P and H_C, where data sets are ranked by P_{out} and Q_f in Figures 2a and 2b, respectively. This result shows that increasing R_P causes Δf to increase, has no influence on f_p, and thus causes Q_f to decrease at both maximum P_{out} and maximum Q_f. Our data also shows that increasing H_C causes Δf to decrease and f_p to increases, and therefore, causes Q_f to increase. The dependence of Δf on R_P is the result of an increase in phase noise due to thermal fluctuations and is a predicted trend based on the simulation results in Ref. 23. Additionally, the decrease in Δf and the increase in Q_f with H_C confirms the experiment results presented in Ref. 24 since a larger H_C indicates a larger shape anisotropy. The key observation in our results is that both Δf and Q_f had a much stronger correlation with H_C than with R_P, as seen from the relative magnitudes of ρ. This suggests that decreases in signal quality due to reduction in STO size can be easily mitigated if the aspect ratio is designed to maximize device coercivity.

Our analysis also shows that increasing R_P causes decreases in H_{bias} and I_{bias} at both maximum P_{out} and Q_f, as seen in Figures 2a and 2b, which implies a reduction in energy consumption when operating at maximum P_{out} and Q_f. On the other hand, these figures show that increasing H_C causes H_{bias} and I_{bias} to increase. Again, these results are not surprising since a larger coercivity indicates larger thermal stability. However, the important findings from our data are revealed through the correlation coefficients, which show that I_{bias} has a stronger correlation with R_P than with H_C, meaning that I_{bias} will likely decreases as the STO size decreases, regardless of the devices coercivity. Alternatively, H_{bias} has a slightly stronger correlation with H_C than with R_P, however, this is not necessarily a detrimental effect since larger H_{bias} does not necessarily mean larger applied field. Recall that H_{bias} also considered H_{stray}, which means that increases in H_{bias} do not need to be compensated by R_P, but rather by a stray field with the correct orientation. In fact, several of the STOs in our study generated precession signals at zero-applied fields (see supplementary material, note 4).

The correlation between R_P and P_{out} is quite insignificant, however H_C is noticeably correlated with reductions P_{out}. The cause of this effect is most likely due to device failure in our experiment and does not represent the influence of H_C on P_{out}. Since STOs with larger H_C require I_{bias}, they are more susceptible to device failure caused by breakdown in MgO tunneling barrier. In our experiment, many of our devices failed at $I_{bias} \approx 300 - 350$ μA. This was not an issue for STOs with $R_P \geq 3k\Omega$ and/or $H_C \leq 20$ Oe since maximum P_{out} was achieved at bias currents well below 300 μA. However, those devices with $H_C > 50$ Oe may have failed at I_{bias} below its maximum P_{out} capability. Since it is questionable if maximum P_{out} was achieved in STOs with $H_C > 50$ Oe, any relation observed for H_C versus P_{out} are not conclusive. However, from a practical point of view, these correlations should not be disregarded since they illustrate that device failure is another factor that should be considered when increasing H_C.

The overall trends observed in Figures 2a and 2b are in good agreement, however, Figure 2c suggests that there are some noticeable discrepancies. Figure 2c shows the correlations in difference between the H_{bias}, I_{bias}, P_{out}, and Q_f values between maximum P_{out} and Q_f (represented as ΔH_{bias}, ΔI_{bias}, ΔP_{out}, and ΔQ_f respectively) with R_P and H_C (see supplementary material, note 5 and supplementary material, Figure 6). This plot shows that R_P causes both ΔH_{bias} and ΔI_{bias} to decrease and H_C causes both ΔH_{bias} and ΔI_{bias} to increase. The ρ values displayed in Figure 2c shows that ΔH_{bias} has a much stronger correlation with H_C than with R_P, whereas ΔI_{bias} has a stronger correlation with R_P. However, the correlation coefficients for ΔI_{bias} with both R_P and H_C are too small to be conclusive on their relative influence.

The data in Figure 2c shows that ΔQ_f decreases with R_P but has a stronger correlation to increases with H_C. Recall that increasing H_C leads to improved maximum Q_f; however, the correlation between

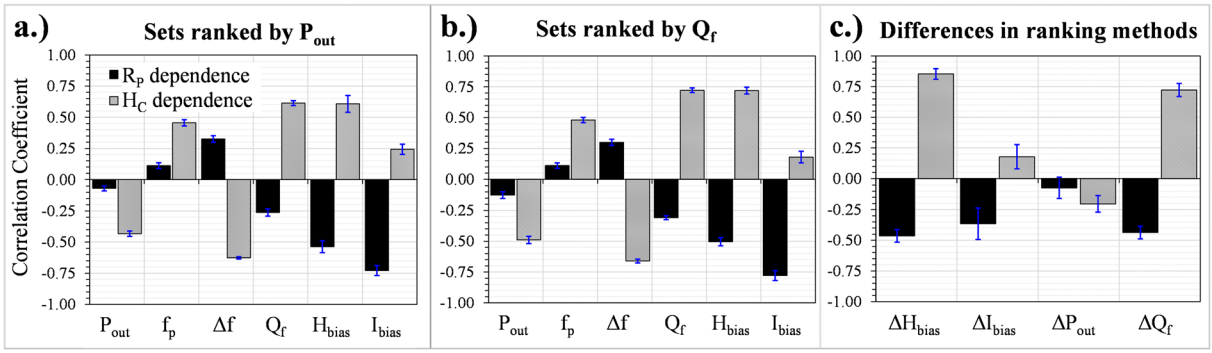

FIG. 2. a-b.) Correlation coefficients for output power (P_{out}), frequency (f_p), linewidth (Δf), quality factor (Q_f), bias field (H_{bias}), and bias current (I_{bias}) with R_P (solid black bars) and H_C (light shaded bars) when data sets are ranked by a.) P_{out} and b.) Q_f. c.) Correlation coefficients for the differences in H_{bias}, I_{bias}, P_{out}, and Q_f between the two methods of ranking data sets (ΔH_{bias}, ΔI_{bias}, ΔP_{out}, and ΔQ_f, respectively).

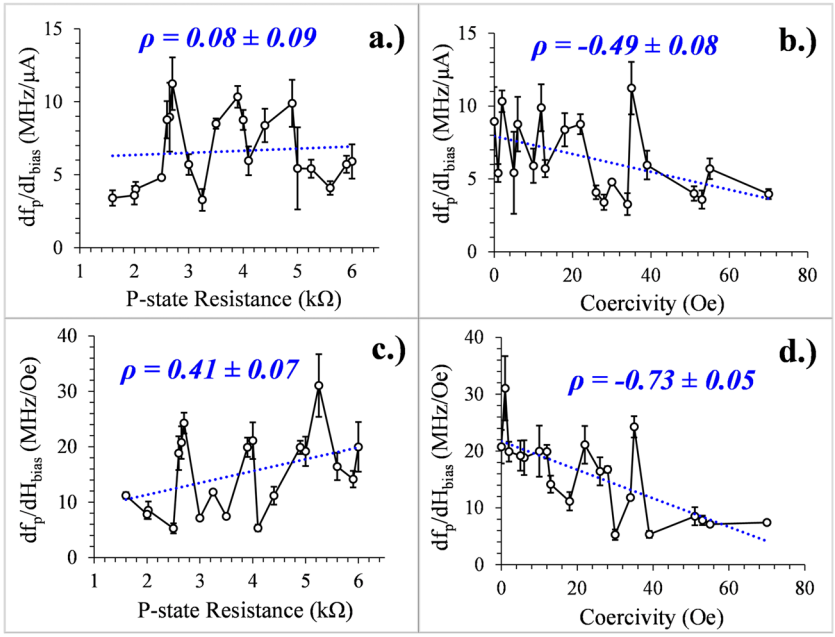

FIG. 3. Frequency slope with respect to a-b.) bias current and c-d.) bias field, represented as df_p/dI_{bias} and df_p/dH_{bias}, respectively. Both metrics are plotted with respect to a, c.) P-state resistance and b, d.) Coercivity.

ΔQ_f and H_C indicates that some signal quality will be sacrificed when operating maximum P_{out} for STOs with high H_C. It should be noted that H_C still has a relatively strong, positive correlation with Q_f at maximum P_{out} ($\rho > 0.6$), which suggests that STOs with high H_C will still produce signals with higher Q_f values at maximum P_{out} than STOs with lower H_C, despite the increase in ΔQ_f. The correlation coefficients for ΔP_{out} suggest that ΔP_{out} does not have a strong dependence on either R_P or H_C. The lack of dependence of ΔP_{out} on R_P is an important feature in terms of device size scaling since it suggests that reducing STO size will not cause further reductions in P_{out} when operating at maximum Q_f. Our data indicates that ΔP_{out} also has a weak correlation H_C, however, the actual dependence on H_C may be misleading since we suspect that maximum P_{out} was not achieved due to device failure for STOs with $H_C > 50$ Oe.

The final two STO performance metrics investigated are the frequency slopes with H_{bias} and I_{bias} (df_p/dH_{bias} and df_p/dI_{bias}, respectively). Note that large df_p/dH_{bias} is a crucial feature for STO read-head sensors and bio-sensors, as well as for components in neural oscillating networks, where STOs interact through dipole interactions.[21] Figure 3a shows that R_P has no significant correlation with df_p/dI_{bias} while Figure 3b shows that H_C causes df_p/dI_{bias} to decrease with a noticeable correlation. Figures 3c–d show that R_P caused df_p/dH_{bias} to increase and H_C caused df_p/dH_{bias} to decrease with much stronger correlations with both R_P and H_C than df_p/dI_{bias}

TABLE I. Summary of the influences of the STOs size and effects on STO performance based on our findings.

	Effects of decreasing STO area	Effects of increasing STO aspect ratio
Advantages	Smaller H_{bias} and I_{bias} required. Decreases ΔH_{bias}, ΔI_{bias}, and ΔQ_f. Larger df_P/dH_{bias}.	Increases signal f_P. Decreases Δf. Increases maximum Q_f.
Neutral effects	No influence on maximum P_{out} and ΔP_{out}. No influence on f_P No influence on df_P/dI_{bias}	Unclear correlation with maximum P_{out} and ΔP_{out} Weak correlation with ΔI_{bias}.
Disadvantages (avoidable)	Decreases maximum Q_f Increases Δf	Larger H_{bias} and I_{bias} required.
Disadvantages (unavoidable)	None	Increases ΔH_{bias} and ΔQ_f. Smaller df_P/dH_{bias} and df_P/dI_{bias}

had. The correlation coefficients shown on these figures indicate that df_P/dH_{bias} has a much stronger correlation with H_C than with R_P.

An overview of the influence of R_P and H_C on a full spectrum of STO performance metrics based on our findings is shown in Table I. In this table, the effects of increasing R_P are listed in the "Effects of decreasing STO area" column and the effects of increasing H_C are listed in the "Effects of increasing STO aspect ratio" column. Here we list all of the key findings from our analysis on the influences of R_P and H_C and categorize them as either advantages, neutral effects, avoidable disadvantages, or unavoidable disadvantages. The difference between avoidable and unavoidable disadvantages is based on the relative correlation coefficients calculated between R_P and H_C for each performance metric studied.

IV. CONCLUSION

In summary, we analyzed spin-torque oscillations generated from 20 MTJs with shape magnetic anisotropy. We then studied the influence device size and shape on multiple key STO performance metrics. Our results showed that there were multiple advantages as well as disadvantages of reducing the STO's size and increasing its aspect ratio. This means that changing either size or shape may improve one aspect of the STO's performance, however, this change will be accompanied by a reduction in another aspect of its performance. While the explanation for some of the results presented are unclear at this point, our results still demonstrate all of the trade-offs in STO performances with as well as illustrating the relative magnitude of their effects between two key device parameters. STOs are promising solutions in a variety of novel applications and our analysis could serve as a guide in designing STOs to optimize the performance metric most important for the desired functions.

SUPPLEMENTARY MATERIAL

See supplementary material for device fabrication methods and stack structure, a list of key device properties for our analysis, field switching hysteresis plots for each device tested, and data used to calculate all correlation coefficients and their uncertainties.

ACKNOWLEDGMENTS

This work is supported in part by Seagate Technology and CAPSL, an SRC program sponsored by the NSF through 1739635. Portions of this work were conducted in the Minnesota Nano Center, which is supported by the National Science Foundation through the National Nano Coordinated Infrastructure Network, award number ECCS-2025124. The authors thank the useful discussion with Dr. Pavol Krivosik and Dr. Mark Kief from Seagate Technology.

DATA AVAILABILITY

The data that support the findings of this study are available from the corresponding author upon reasonable request.

REFERENCES

[1]T. Chen, R. K. Dumas, A. Eklund, P. K. Muduli, A. Houshang, A. A. Awad, P. Dürrenfeld, B. G. Malm, A. Rusu, and J. Åkerman, Proceedings of the IEEE **104**, 1919 (2016).
[2]Y. Zhang, Ph.D. thesis, University of Minnesota, 2014.
[3]Z. Zeng, G. Finocchio, and H. Jiang, Nanoscale **5**, 2219 (2013).
[4]Z. Zeng, P. K. Amiri, I. N. Krivorotov, H. Zhao, G. Finocchio, J.-P. Wang, J. A. Katine, Y. Huai, J. Langer, K. Galatsis, K. L. Wang, and H. Jiang, ACS Nano **6**, 6115 (2012).
[5]Y. Zhang, H. Zhao, A. Lyle, P. A. Crowell, and J.-P. Wang, Appl. Phys. Lett. **100**, 032405 (2012).
[6]A. M. Deac, A. Fukushima, H. Kubota, H. Maehara, Y. Suzuki, S. Yuasa, Y. Nagamine, K. Tsunekawa, D. D. Djayaprawira, and N. Watanabe, Nature Physics **4**, 803 (2008).
[7]A. Hamadeh, Ph.D. thesis, Université Paris Sud–Paris XI, 2014.
[8]W. H. Rippard, M. R. Pufall, S. Kaka, S. E. Russek, and T. J. Silva, Phys. Rev. Lett. **92**, 027201 (2004).
[9]H. S. Choi, S. Y. Kang, S. J. Cho, I.-Y. Oh, M. Shin, H. Park, C. Jang, B.-C. Min, S.-I. Kim, S.-Y. Park, and C.-S. Park, Scientific Reports **4**, 5486 (2014).
[10]S. A. Wolf, A. Y. Chtchelkanova, and D. M. Treger, IBM J. Res. and Dev., **50**, 101 (2006).
[11]P. M. Braganca, B. A. Gurney, B. A. Wilson, J. A. Katine, S. Maat, and J. R. Childress, Nanotechnology **21**, 235202 (2010).
[12]H. Suto, T. Nagasawa, K. Kudo, K. Mizushima, and R. Sato, Appl. Phys. Express **4**, 013003 (2011).
[13]T. Srimani, B. Manna, A. K. Mukhopadhyay, K. Roy, and M. Sharad, in 2016 74th Annual Device Research Conference (DRC), Newark, DE, 2016.
[14]S. Urazhdin and P. Tabor, Phys. Rev. Lett. **105**, 104101 (2010).
[15]W. H. Rippard, M. R. Pufall, S. Kaka, T. J. Silva, S. E. Russek, and J. A. Katine, Phys. Rev. Lett. **95**, 067203 (2005).
[16]S. Kaka, M. R. Pufall, W. H. Rippard, T. J. Silva, S. E. Russek, and J. A. Katine, Nature **437**, 389 (2005).
[17]N. Locatelli, A. Hamadeh, F. Abreu Araujo, A. D. Belanovsky, P. N. Skirdkov, R. Lebrun, V. V. Naletov, K. A. Zvezdin, M. Muñoz, J. Grollier, O. Klein, V. Cros, and G. de Loubens, Scientific Reports **5**, 17039 (2015).
[18]R. Lebrun, S. Tsunegi, P. Bortolotti, H. Kubota, A. S. Jenkins, M. Romera, K. Yakushiji, A. Fukushima, J. Grollier, S. Yuasa, and V. Cros, Nature Communications **8**, 15825 (2017).
[19]D. E. Nikonov, G. Csaba, W. Porod, T. Shibata, D. Voils, D. Hammerstrom, I. A. Young, and G. I. Bourianoff, IEEE J. Explor. Solid-State Comput. Devices Circuits **1**, 85 (2015).
[20]M. R. Pufall, W. H. Rippard, G. Csaba, D. E. Nikonov, G. I. Bourianoff, and W. Porod, IEEE J. Explor. Solid-State Comput. Devices Circuits **1**, 76 (2015).
[21]K. Yogendra, D. Fan, and K. Roy, IEEE Trans. Magn. **51**, 4003909 (2015).
[22]J. Torrejon, M. Riou, F. A. Araujo, S. Tsunegi, G. Khalsa, D. Querlioz, P. Bortolotti, V. Cros, K. Yakushiji, A. Fukushima, H. Kubota, S. Yuasa, M. D. Stiles, and J. Grollier, Nature **547**, 428 (2017).
[23]X. Chao, M. Jamali, and J.-P. Wang, AIP Advances **7**, 056624 (2017).
[24]X. Chao, M. Jamali, and J.-P. Wang, AIP Advances **10**, 045101 (2020).